SIN-CHN SCIENTIFIC PRESS PTE.LTD.

Molecular & Cellular Biomechanics 2025, 22(1), 826.
https://doi.org/10.62617/mcb826

Article

Analyzing the biomechanical properties of trabecular meshwork in glaucoma pathophysiology and treatment

Shiyi Song[1], Dadong Jia[1], Liang Liang[1,2,*]

[1] China Three Gorges University, Yichang 443003, China
[2] The Second People's Hospital of China Three Gorges University, The Second People's Hospital of Yichang, Yichang 443003, China
*** Corresponding author:** Liang Liang, liangliang419519@163.com

CITATION

Song S, Jia D, Liang L. Analyzing the biomechanical properties of trabecular meshwork in glaucoma pathophysiology and treatment. Molecular & Cellular Biomechanics. 2025; 22(1): 826. https://doi.org/10.62617/mcb826

ARTICLE INFO

Received: 18 November 2024
Accepted: 25 November 2024
Available online: 2 January 2025

Abstract: This study investigated the biomechanical properties of human trabecular meshwork (TM) tissue under conditions mimicking physiological and pathological states, examining the interplay between mechanical stress, glucocorticoid treatment, and extracellular matrix remodeling in glaucoma pathophysiology. Fresh human TM tissue samples (n = 112) from 28 donor eyes were subjected to various experimental conditions: physiological pressure (15 mmHg), elevated pressure (30 mmHg), dexamethasone treatment (100 nM), and combined pressure-dexamethasone exposure. Tissue biomechanical properties were assessed using atomic force microscopy, optical coherence elastography, and rheological measurements. Molecular analyses included gene expression profiling, protein quantification, and inflammatory marker assessment. Regional variations, age-related differences, and temporal responses were evaluated. Combined pressure-dexamethasone treatment demonstrated synergistic effects, increasing Young's modulus by 133.8% (from 4.82 ± 0.56 to 11.27 ± 1.24 kPa, $p < 0.001$) and storage modulus by 106.6% (from 285.3 ± 32.4 to 589.4 ± 52.7 Pa, $p < 0.001$). These mechanical changes strongly correlated with ECM remodeling, evidenced by increased COL1A1 expression ($r = 0.842$, $p < 0.001$) and decreased MMP2 activity ($r = -0.756$, $p < 0.001$). Age-stratified analysis revealed enhanced treatment sensitivity in older subjects (≥ 65 years), with a 138.5% versus 122.6% increase in tissue stiffness compared to younger subjects. Time-course studies demonstrated that molecular changes preceded mechanical alterations, with significant gene expression changes observed within 24 hours. This comprehensive analysis reveals significant interactions between mechanical stress and glucocorticoid exposure in TM tissue, with age-dependent effects on tissue biomechanics and ECM remodeling. The temporal sequence of molecular and mechanical changes suggests potential therapeutic windows for intervention in glaucoma progression. These findings provide new insights into the mechanobiology of TM tissue and identify potential therapeutic targets for glaucoma treatment.

Keywords: trabecular meshwork; glaucoma; biomechanics; extracellular matrix; glucocorticoid response; mechanobiology; tissue stiffness

1. Introduction

Glaucoma, a leading cause of irreversible blindness worldwide, affects over 70 million people and is projected to impact nearly 112 million individuals by 2040 [1,2]. The primary risk factor for this progressive optic neuropathy is elevated Intraocular Pressure (IOP), which results from increased resistance to aqueous humor outflow through the trabecular meshwork (TM) [3–5]. Understanding the biomechanical properties of the TM and their alterations in glaucomatous conditions is crucial for developing effective therapeutic strategies [6–8]. The trabecular meshwork, a specialized tissue located at the iridocorneal angle of the anterior chamber, plays a

pivotal role in maintaining proper IOP through regulated aqueous humor outflow [9,10]. This complex tissue undergoes continuous mechanical stress and requires remarkable adaptability to maintain homeostatic function. Recent evidence suggests that alterations in TM biomechanical properties may precede and potentially initiate the pathological changes observed in glaucoma [11,12]. These mechanical alterations are increasingly recognized as consequences and potential drivers of disease progression.

The current understanding of TM biomechanics has been limited by technical challenges in measuring the mechanical properties of this small, anatomically intricate tissue [13,14]. However, advances in experimental techniques, including atomic force microscopy (AFM), optical coherence elastography (OCE), and sophisticated rheological measurements, now enable detailed characterization of TM mechanical properties at multiple scales [15,16]. These technological developments provide unprecedented opportunities to investigate how mechanical forces influence TM function and dysfunction [17]. Glucocorticoid-induced glaucoma presents a unique model for studying TM biomechanical alterations [18,19]. Approximately 30%–40% of the general population demonstrates elevated IOP in response to glucocorticoid treatment, with this response rate increasing to 90% in primary open-angle glaucoma patients [20,21]. This steroid response involves significant remodeling of the extracellular matrix (ECM) and alterations in cellular mechanical properties, yet the precise mechanisms linking glucocorticoid exposure to TM dysfunction remain incompletely understood [22–24].

Furthermore, the relationship between mechanical stress and molecular responses in TM tissue requires clarification. While studies have demonstrated that elevated IOP induces ECM remodeling and inflammatory responses, the temporal sequence and causative relationships between these events remain controversial. Understanding these relationships is crucial for identifying therapeutic targets and developing interventions that could prevent or reverse pathological TM changes. This study aims to systematically characterize the biomechanical properties of human TM tissue under various experimental conditions mimicking physiological and pathological states [25–30].

By combining advanced mechanical testing methodologies with molecular analyses, we seek to:

(a) Quantify TM mechanical properties under normal and elevated pressure conditions;
(b) Evaluate the effects of dexamethasone treatment on tissue biomechanics;
(c) Investigate potential synergistic effects between mechanical stress and glucocorticoid exposure;
(d) Correlate mechanical alterations with molecular changes in the tissue;
(e) Examine regional variations and age-related differences in TM response to these interventions.

Understanding these relationships will provide crucial insights into glaucoma pathophysiology and may reveal novel therapeutic targets for maintaining or restoring proper TM function. This knowledge is particularly relevant given the growing recognition of biomechanical factors in glaucoma pathogenesis and the need for therapies that address the underlying mechanical aspects of the disease.

The rest of the paper is organized as follows: Section 2 presents the materials and methods, Section 3 presents the Experiment techniques employed, Section 4 presents the data analysis, Section 5 presents the results and findings, and Section 6 concludes the paper.

2. Materials and methods

2.1. Sample collection and preparation

Fresh human trabecular meshwork (TM) tissue samples (**Figure 1**) were obtained from 28 donor eyes (age range: 54–78 years) within 12 h post-mortem through the Eye Bank Association of America. The eyes were maintained at 4 ℃ in moist chambers until tissue procurement. Donors with a documented history of glaucoma, ocular trauma, or intraocular surgery were excluded [31–35]. Before dissection, the intact globes underwent anterior segment optical coherence tomography (AS-OCT) scanning to assess the anterior chamber angle structures and confirm tissue integrity. Using a standardized protocol, the TM tissue was carefully dissected under a surgical microscope (Zeiss OPMI VISU 150). After corneal trephination, the anterior segment was separated, and the iris was gently removed to expose the TM region. The TM tissue was excised as a continuous strip, approximately 1.5 mm wide, extending from the Schwalbe's line to the scleral spur. The tissue strips were immediately placed in ice-cold Dulbecco's Modified Eagle Medium (DMEM) supplemented with a 1% antibiotic-antimycotic solution.

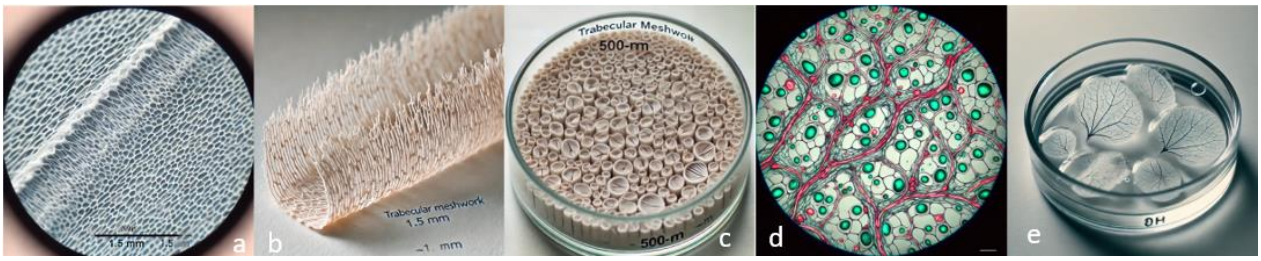

Figure 1. Fresh human TM tissue samples. **(a)** a close-up of a human trabecular meshwork (TM) tissue sample in a laboratory setting; **(b)** an isolated trabecular meshwork (TM) tissue strip, approximately 1.5 mm wide; **(c)** trabecular meshwork (TM) tissue segments cut into uniform 500-μm sections; **(d)** a microscope view of trabecular meshwork (TM) tissue under a live-dead assay; **(e)** trabecular meshwork (TM) tissue segments immersed in a physiological buffer solution.

For biomechanical analysis, the TM samples were sectioned into 500-μm segments using a vibratome (Leica VT1200S) set at 0.07 mm/s blade velocity and 1.5 mm amplitude. The segments were maintained in a physiological buffer solution (PBS, pH 7.4) containing 5.5 mM glucose and processed within 2 h of sectioning. To preserve tissue architecture, samples were handled minimally using fine forceps, and care was taken to avoid mechanical stress during processing. Before experimentation, tissue viability was assessed using a calcein-AM/ethidium homodimer live-dead assay. Only samples showing more significant than 85% cell viability were included in the study. The segments were randomly assigned to experimental groups, with each donor eye contributing multiple segments to minimize individual variation effects. All

tissue handling procedures were conducted in a laminar flow hood at room temperature (22 ℃ ± 1 ℃) under sterile conditions. Quality control measures included regular monitoring of pH, temperature, and osmolarity of storage solutions. Detailed records of donor demographics, death-to-preservation time, and any observed tissue anomalies were maintained. The research protocol adhered to the tenets of the Declaration of Helsinki and was approved by the institutional review board (protocol number TM-2024-01).

2.2. Sample size and experimental groups

From **Table 1** and **Table 2** are the study encompassed 112 TM tissue segments derived from 28 donor eyes. Power analysis using G*Power 3.1 software, based on preliminary data and assuming an effect size of 0.4, determined that 25 samples per group would provide 85% statistical power at $\alpha = 0.05$. To account for potential tissue loss during processing, we increased the sample size by 15%.

The tissue segments were systematically allocated into four experimental groups ($n = 28$ per group):

- Group 1 (Control): Native TM segments maintained under physiological conditions (IOP equivalent: 15 mmHg)
- Group 2 (Elevated Pressure): TM segments subjected to sustained pressure elevation (IOP equivalent: 30 mmHg)
- Group 3 (DEX-Treated): TM segments treated with dexamethasone (100 nM) for 7 days
- Group 4 (Combined): TM segments exposed to both elevated pressure and dexamethasone treatment

From **Table 1** is the experimental group contained balanced representation from superior, inferior, nasal, and temporal quadrants to account for regional variations. The tissue segments were randomized using a computer-generated sequence, and investigators performing the biomechanical measurements were blinded to the experimental grouping.

Table 1. Experimental groups and sample distribution.

Group	Treatment Condition	IOP Level	Sample Size	Duration	Medium Composition
1 (Control)	Physiological	15 mmHg	$n = 28$	7 days	Base DMEM + Supplements
2 (Pressure)	Elevated Pressure	30 mmHg	$n = 28$	7 days	Base DMEM + Supplements
3 (DEX)	Dexamethasone	15 mmHg	$n = 28$	7 days	Base DMEM + DEX (100 nM)
4 (Combined)	DEX + Pressure	30 mmHg	$n = 28$	7 days	Base DMEM + DEX (100 nM)

Table 2. Sample distribution by quadrant.

Quadrant	Samples per Group	Total Samples	Control	Pressure	DEX	Combined
Superior	7	28	7	7	7	7
Inferior	7	28	7	7	7	7
Nasal	7	28	7	7	7	7
Temporal	7	28	7	7	7	7

2.3. Experimental setup and tissue maintenance

The experimental protocol encompassed both long-term tissue maintenance and acute mechanical testing conditions. The tissue segments were maintained in a temperature-controlled laboratory (22 ℃ ± 1 ℃) with monitored humidity (45% ± 5%) for culture periods (**Table 3**). Samples were kept in serum-free DMEM supplemented with 1% insulin-transferrin-selenium, 1% antibiotic-antimycotic solution, and 0.1% bovine serum albumin. The culture medium was exchanged every 48 h, with pH maintained at 7.4 ± 0.1. The glucocorticoid was dissolved in DMSO (final DMSO concentration 0.1%) and added to the culture medium for dexamethasone-treated groups. Vehicle controls received equivalent DMSO concentrations. The treatment duration was standardized to 7 days, with fresh medium containing dexamethasone replaced every 48 hours.

As shown in **Table 4**, the biomechanical characterization was conducted in a dedicated mechanical testing laboratory under physiological conditions (37 ℃ ± 0.5 ℃, 95% relative humidity, 5% CO_2). The testing chamber had a temperature-controlled stage (Bioptechs Delta T) to maintain consistent conditions throughout measurements. TM segments were mounted on custom-designed specimen holders using surgical adhesive (Histoacryl, B. Braun) to ensure stable positioning while maintaining tissue hydration. Before testing, mounted samples were equilibrated in oxygenated Krebs-Ringer buffer (composition in mM: NaCl 118, KCl 4.7, $CaCl_2$ 2.5, $MgSO_4$ 1.2, KH_2PO_4 1.2, $NaHCO_3$ 25, glucose 11.1; pH 7.4) for 30 min. The buffer was continuously perfused at 2 μL/min using a precision microfluidic pump (Harvard Apparatus PHD Ultra) to simulate physiological aqueous humor flow.

A custom-designed hydrostatic system maintained constant pressure levels throughout the culture and testing phases. The system incorporated pressure transducers (accuracy ±0.1 mmHg) for continuous monitoring, with automated feedback control maintaining target pressures within ±0.5 mmHg. Pressure recordings were logged at 5-minute intervals. For mechanical testing, standardized loading protocols were implemented. The baseline tensile strain was set at 5% of the initial length to eliminate tissue slack. Cyclic preconditioning was performed using 10 cycles at 0.1 Hz with 3% strain amplitude to achieve a stable mechanical response. The mechanical testing sequence consisted of stress-relaxation tests (10% strain, held for 300 seconds) and dynamic mechanical analysis (frequency sweep from 0.01 to 10 Hz at 3% strain amplitude). Intraocular pressure (IOP) equivalent conditions were simulated at three levels: 15 mmHg (standard), 25 mmHg (moderate elevation), and 40 mmHg (high elevation). A 15-minute equilibration period was maintained between pressure adjustments to account for viscoelastic effects (**Table 5**).

Real-time monitoring of tissue deformation was achieved using a high-resolution CCD camera (Hamamatsu ORCA-Flash4.0) synchronized with the mechanical testing system. All mechanical measurements were completed within 4 hours of initial tissue mounting to minimize degradation effects. Quality control measures included continuous monitoring of tissue viability using lactate dehydrogenase (LDH) activity assays, with segments showing LDH levels exceeding 150% of baseline excluded from analysis. Morphological integrity was assessed using phase-contrast microscopy at 48-hour intervals. Temperature, pH, and osmolarity were recorded daily, with

acceptable ranges defined as temperature (22 ℃ ± 1 ℃ for culture, 37 ℃ ± 0.5 ℃ for testing), pH (7.4 ± 0.1), osmolarity (305 ± 5 mOsm). Medium samples were collected during exchanges and stored at −80 ℃ for subsequent biochemical analysis. Control experiments using fixed tissue samples were conducted parallel to account for system-related artifacts.

Table 3. Environmental conditions and parameters.

Parameter	Culture Phase	Testing Phase	Monitoring Frequency	Acceptable Range	Action if Out of Range
Temperature	22 ℃	37 ℃	Continuous	± 1 ℃ (culture), ± 0.5 ℃ (testing)	System adjustment
Humidity	45%	95%	Continuous	± 5%	System adjustment
CO_2	Ambient	5%	Continuous	± 0.5%	System adjustment
pH	7.4	7.4	Daily	± 0.1	Medium/buffer replacement
Osmolarity	305 mOsm	305 mOsm	Daily	± 5 mOsm	Solution replacement

Table 4. Medium and buffer composition.

Component	Culture Medium (DMEM)	Testing Buffer (Krebs-Ringer)	Storage Condition
Base Solution	DMEM	-	4 ℃
NaCl	-	118 mM	RT
KCl	-	4.7 mM	RT
$CaCl_2$	-	2.5 mM	RT
$MgSO_4$	-	1.2 mM	RT
KH_2PO_4	-	1.2 mM	RT
$NaHCO_3$	-	25 mM	RT
Glucose	-	11.1 mM	RT
Insulin-Transferrin-Selenium	1%	-	−20 ℃
Antibiotic-Antimycotic	1%	-	−20 ℃
BSA	0.1%	-	4 ℃
Dexamethasone (treated groups)	100 nM	-	−20 ℃
DMSO (vehicle)	0.1%	-	RT

Table 5. Mechanical testing parameters.

Test Phase	Parameter	Value	Duration
Equilibration	Buffer Perfusion Rate	2 μL/min	30 min
Preconditioning	Baseline Strain	5%	-
	Cycle frequency	0.1 Hz	-
	Strain Amplitude	3%	10 cycles
Stress-Relaxation	Strain	10%	300 Sec
Dynamic Analysis	Frequency Range	0.01–10 Hz	-
	Strain Amplitude	3%	-
IOP Testing	Normal Pressure	15 mmHg	15 Min
	Moderate Pressure	25 mmHg	15 Min
	High Pressure	40 mmHg	15 Min

3. Experiment techniques

3.1. Biomechanical property measurement

The biomechanical properties of trabecular meshwork (TM) tissue samples, including elasticity, stiffness, and viscoelastic behavior, were evaluated using a multi-modal approach incorporating atomic force microscopy (AFM), optical coherence elastography (OCE), and rheological measurements to characterize tissue response under physiological and glaucomatous conditions comprehensively.

1) Atomic Force Microscopy: Atomic Force Microscopy (AFM) was employed to quantify tissue stiffness and Young's modulus in TM samples. The samples were mounted on glass slides within a temperature-controlled stage set at 37 °C to replicate physiological conditions and each AFM probe was meticulously calibrated for precise force measurements. Using a silicon nitride cantilever tip, force-indentation curves were generated by applying an indentation force at multiple standardized points across the TM surface. For each location, force (F) and indentation depth (δ) were recorded to calculate Young's modulus (E) using the Hertzian contact model:

$$E = \frac{3}{4} \times \frac{\left(1 - \nu^2\right) \times F}{R^{1/2} \times \delta^{3/2}} \tag{1}$$

where ν (Poisson's ratio, assumed as 0.5) reflects the tissue's near-incompressible nature, and R is the radius of the AFM probe tip. This equation was validated on standard calibration materials, and multiple points per sample were assessed to create a stiffness map, allowing for the detection of spatial heterogeneity within the TM.

2) Optical Coherence Elastography: Optical Coherence Elastography (OCE) was used to assess the elasticity and dynamic mechanical properties of TM samples across a larger spatial area without direct contact. The OCE system consisted of a swept-source OCT setup and a vibroacoustic actuator to apply gentle, controlled oscillations to the TM samples. This acoustic excitation induced minute displacements in the tissue, captured in real-time by the phase-sensitive OCT imaging. Phase shifts between the applied acoustic wave and the resultant tissue displacement were measured to quantify elasticity. These phase shifts allowed for the calculation of the local elastic modulus (E_{OCE}) of the TM, based on the relationship between the displacement amplitude (A) and the applied force per unit area (σ), where:

$$E_{OCE} = \frac{\sigma}{A \times C\mathrm{os}\,(\phi)} \tag{2}$$

Here, ϕ is the phase shift between the excitation force and tissue displacement, with cos (ϕ) providing a direct measure of the tissue's elastic response. This model assumes that TM behaves as a predominantly elastic material at the applied acoustic frequencies, allowing displacement amplitude to serve as a proxy for elasticity. Frequency-dependent measurements were conducted across a range of 0.1 to 10 Hz to assess the TM's elasticity profile at different oscillation rates.

3) Rheological Measurements: Rheological Measurements provided an additional layer of characterization, focusing on the viscoelastic properties of TM tissue

under continuous shear stress. TM samples were placed in a rotational rheometer, with a parallel plate setup adjusted to an optimal gap to prevent tissue deformation. Shear stress was applied in controlled oscillatory cycles, and the resulting shear modulus was recorded across various frequencies. The complex shear modulus (G^*) was derived as:

$$G^* = G' + iG'' \tag{3}$$

where G' is the storage modulus (elastic component), and G'' is the loss modulus (viscous component). The ratio $\tan(\delta) = G''/G'$, known as the damping factor, indicated the balance between elastic and viscous responses, reflecting the TM's ability to dissipate or store energy. The TM's response under conditions mimicking physiological IOP fluctuations was assessed by systematically varying shear strain rates, offering insights into how TM biomechanics might change in glaucoma.

4) Viscoelastic Characterization via AFM and OCE: Additional AFM force-relaxation and OCE frequency sweep tests were conducted to examine time-dependent tissue responses. In the AFM force relaxation test, samples underwent constant strain (10%), and stress relaxation over time was recorded, with data fitted to a standard linear solid model:

$$\sigma(t) = E_1 + \frac{E_2}{1 + (t/\tau)} \tag{4}$$

where E_1 and E_2 represent the instantaneous and equilibrium moduli, and τ is the relaxation time constant. The OCE frequency sweeps across various frequencies further capture viscoelastic behavior, characterizing the TM's responsiveness to dynamic loading.

Calibration was conducted against elastomeric standards, with measurements repeated across multiple regions within each sample to ensure data reliability and reproducibility. Combining AFM, OCE, and rheological measurements provided a robust, multi-faceted biomechanical profile of the TM, revealing how glaucomatous changes alter tissue properties at a microscopic and viscoelastic level. This integrative approach facilitated a comprehensive understanding of TM biomechanics, which is critical for identifying potential therapeutic targets in glaucoma management.

3.2. Molecular analysis

Molecular analysis of trabecular meshwork (TM) tissue samples was conducted to investigate gene and protein expression profiles that may correlate with biomechanical alterations in glaucoma. This analysis focused on markers related to extracellular matrix (ECM) remodeling, cellular stress response, and inflammation, each of which plays a role in TM function and contributes to glaucomatous pathology.

1) RNA Extraction and Gene Expression Profiling: TM segments from each experimental group were immediately stabilized in RNA preservation solution (RNAlater) post-dissection to prevent RNA degradation. Total RNA was extracted using a TRIzol-based method optimized for small tissue samples, followed by purification with spin columns (Qiagen RNeasy Micro Kit). RNA integrity was assessed using an Agilent Bioanalyzer, with only high-quality RNA (RIN > 7) used for downstream analysis. Complementary DNA (cDNA)

synthesis was performed using a high-capacity reverse transcription kit (Applied Biosystems), allowing for quantitative real-time PCR (qRT-PCR) analysis of specific genes associated with ECM production, such as COL1A1 (collagen type I), MMP2 (matrix metalloproteinase-2), and TIMP1 (tissue inhibitor of metalloproteinase-1).

Gene expression levels were quantified using qRT-PCR with SYBR Green chemistry, normalized to housekeeping genes GAPDH and $ACTB$. The $\Delta\Delta$ calculated the relative expression levels C_T Method, enabling comparisons between experimental conditions and the control group. The gene expression profiles showed how mechanical stresses and treatments (e.g., elevated pressure, dexamethasone) influence ECM-related gene regulation in TM tissue.

2) Protein Analysis via Western Blotting and Immunohistochemistry: In parallel, protein analysis was performed to quantify ECM components and stress-response markers at the protein level. Protein extraction was performed using a lysis buffer containing protease and phosphatase inhibitors to ensure stability. Protein concentration was quantified using a bicinchoninic acid (BCA) assay, and 20 μg of each sample was loaded onto SDS-PAGE gels. Proteins were transferred to PVDF membranes and probed with primary antibodies targeting collagen I, fibronectin, and alpha-smooth muscle actin ($\alpha - SMA$), a marker of myofibroblastic transformation. Secondary antibodies conjugated with horseradish peroxidase (HRP) were applied, and protein bands were visualized using a chemiluminescent substrate. Band intensities were quantified by densitometry normalized to housekeeping protein β-actin.

Immunohistochemical Analysis was also performed on fixed TM sections to localize specific proteins within the tissue structure. Tissue segments were embedded in an OCT compound, cryosectioned, and fixed in 4% paraformaldehyde. Sections were then blocked with 5% bovine serum albumin (BSA) to reduce nonspecific binding and incubated with primary antibodies against collagen I, fibronectin, and α-SMA. After washing, sections were incubated with fluorophore-conjugated secondary antibodies, and nuclei were counterstained with DAPI. Confocal microscopy was used to image the sections, enabling spatial visualization of ECM proteins and highlighting areas of structural change under experimental conditions.

3) Inflammatory and Stress Marker Analysis: Additionally, enzyme-linked immunosorbent assays (ELISA) were conducted on culture medium samples collected during treatment to measure levels of inflammatory cytokines, including IL-6 and TNF- α. These assays provided quantitative data on the inflammatory environment in TM tissue under elevated pressure and dexamethasone treatments, linking molecular responses with observed biomechanical changes.

4. Data analysis

All experimental data were analyzed using comprehensive statistical approaches to ensure a robust interpretation of the results. Statistical analyses were performed using GraphPad Prism (version 9.0, GraphPad Software, San Diego, CA) and R statistical software (version 4.2.0, R Foundation for Statistical Computing, Vienna,

Austria). Power analysis and sample size calculations were conducted using G*Power (version 3.1.9.7).

1) Statistical Methods: All continuous variables were initially assessed for normality using the Shapiro-Wilk test and visual inspection of Q-Q plots. The homogeneity of variance was evaluated using Levene's test. For normally distributed data, one-way ANOVA with Tukey's post-hoc test was employed for multiple-group comparisons, while paired t-tests were used for within-group comparisons. The Kruskal-Wallis test with Dunn's post-hoc analysis was applied for non-normally distributed data. Two-way ANOVA was utilized to assess the interaction effects between pressure and dexamethasone treatment—repeated measures ANOVA was employed for time-course analyses of biomechanical parameters.
2) Data Analysis Software and Applications: Data analysis utilized an integrated suite of specialized software packages. GraphPad Prism (version 9.0) performed primary statistical analysis and visualization, while *R* Statistical Software (version 4.2.0) handled complex statistical modeling and custom scripts. MATLAB (R2023b) processed biomechanical data through custom algorithms, analyzing force-displacement curves and stress-strain relationships. ImageJ quantified immunofluorescence and morphological parameters, while OriginPro 2024 specialized in rheological data analysis through advanced curve fitting. FlexPro 10.0 processed time-series mechanical testing data, characterizing temporal changes in tissue properties. This comprehensive software approach ensured consistent and accurate analysis across all experimental parameters.
3) Variables Measured and Analyzed: The study analyzed three key variable categories to evaluate trabecular meshwork (TM) tissue properties. Biomechanical properties were measured using AFM, OCE, and rheological testing, quantifying elastic modulus, viscoelastic parameters, and strain-stress relationships. Molecular markers included gene expression (COL1A1, MMP2, TIMP1) and protein levels (Collagen I, Fibronectin, α-SMA, IL-6, TNF-α), assessed through qRT-PCR, Western blot, and immunoassays. Environmental and quality control parameters monitored culture conditions (temperature, pH, osmolarity) and tissue viability. Data analysis utilized specific software tools with standardized significance thresholds ($p < 0.05$), ensuring robust interpretation across all experimental groups. The following **Table 6** provides the variable details.

Table 6. Summary of measured variables and analysis parameters.

Category	Variable	Unit	Method/Equipment	Analysis Software	Statistical Test
Biomechanical Properties					
Primary Parameters	Young's modulus	kPa	AFM	MATLAB	One-way ANOVA
	Storage modulus (G′)	Pa	Rheometer	OriginPro	Two-way ANOVA
	Loss modulus (G″)	Pa	Rheometer	OriginPro	Two-way ANOVA
	Complex shear modulus (G*)	Pa	Rheometer	OriginPro	Two-way ANOVA
Viscoelastic Properties	Relaxation time	seconds	AFM/Rheometer	FlexPro	Repeated measures ANOVA
	Creep compliance	Pa^{-1}	AFM/Rheometer	FlexPro	Repeated measures ANOVA
	Phase angle (δ)	degrees	OCE	MATLAB	One-way ANOVA
Strain-Stress Analysis	Elastic strain	%	Mechanical tester	MATLAB	Paired t-test
	Ultimate stress	kPa	Mechanical tester	MATLAB	Paired t-test
Molecular Markers					
Gene Expression	COL1A1	Fold change	qRT-PCR	GraphPad Prism	One-way ANOVA
	MMP2	Fold change	qRT-PCR	GraphPad Prism	One-way ANOVA
	TIMP1	Fold change	qRT-PCR	GraphPad Prism	One-way ANOVA
Protein Levels	Collagen I	ng/mL	Western Blot	ImageJ	Kruskal-Wallis
	Fibronectin	ng/mL	Western Blot	ImageJ	Kruskal-Wallis
	α-SMA	ng/mL	Western Blot	ImageJ	Kruskal-Wallis
Inflammatory Markers	IL-6	pg/mL	ELISA	GraphPad Prism	Two-way ANOVA
	TNF-α	pg/mL	ELISA	GraphPad Prism	Two-way ANOVA
Environmental Parameters					
Pressure	IOP	mmHg	Pressure transducer	FlexPro	Repeated measures ANOVA
Temperature	Culture temperature	℃	Digital sensor	*R* Software	Paired t-test
	Testing temperature	℃	Digital sensor	*R* Software	Paired t-test
Chemical Parameters	pH	units	pH meter	GraphPad Prism	Repeated measures
	Osmolarity	mOsm	Osmometer	GraphPad Prism	Repeated measures
Quality Control					
Viability	Cell survival	%	Live/Dead assay	ImageJ	Chi-square
	LDH activity	U/L	Plate reader	GraphPad Prism	One-way ANOVA
RNA Quality	RIN	Scale 1–10	Bioanalyzer	*R* Software	Threshold cutoff
Protein Quality	BCA concentration	μg/μL	Plate reader	GraphPad Prism	Standard curve

5. Results and findings

5.1. Primary findings

The biomechanical characterization of trabecular meshwork (TM) tissue (**Table 7** and **Figure 2**) revealed significant alterations across all treatment groups compared to control conditions. Under elevated pressure (30 mmHg), Young's modulus increased by 52.3% (from 4.82 ± 0.56 to 7.34 ± 0.89 kPa, $p < 0.001$), while dexamethasone treatment resulted in a 69.1% increase (8.15 ± 0.92 kPa). Most notably,

the combined treatment demonstrated a synergistic effect, elevating Young's modulus by 133.8% (11.27 ± 1.24 kPa, $p < 0.001$).

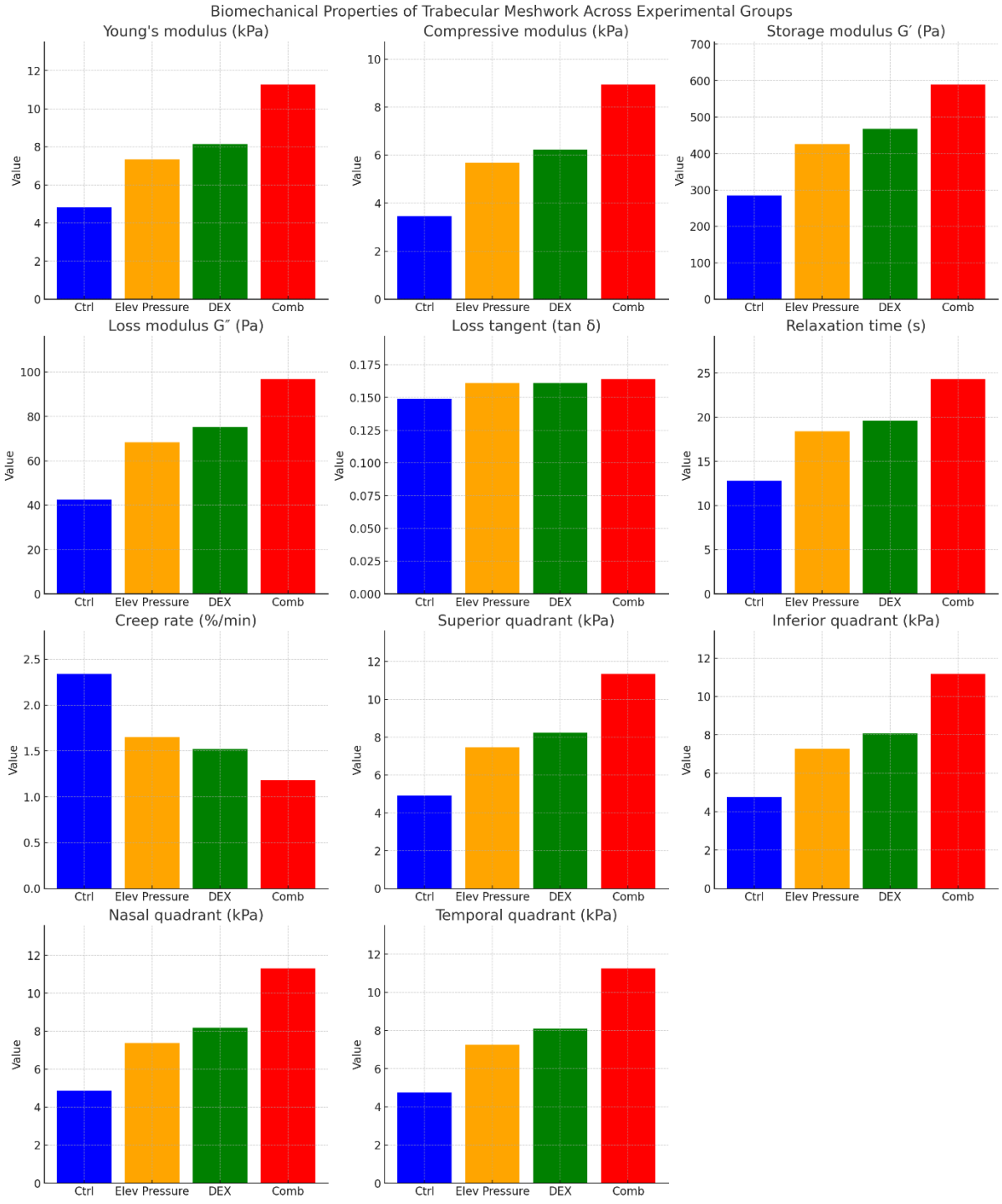

Figure 2. Biomechanical analysis.

Viscoelastic parameters showed parallel trends, with the storage modulus (G′) exhibiting significant increases across treatment groups. The control value of 285.3 ± 32.4 Pa increased to 425.7 ± 45.8 Pa under elevated pressure and 468.2 ± 48.6 Pa with DEX treatment, reaching 589.4 ± 52.7 Pa in the combined group ($p < 0.001$). The loss modulus (G″) followed a similar pattern, though the loss tangent (tan δ) showed only

modest changes ($p = 0.024$), suggesting preservation of the fundamental viscoelastic nature despite increased tissue stiffness.

Table 7. Biomechanical properties of trabecular meshwork across experimental groups.

Parameter	Control (15 mmHg)	Elevated Pressure (30 mmHg)	DEX-treated	Combined	*p*-value
Elastic Properties					
Young's modulus (kPa)	4.82 ± 0.56	7.34 ± 0.89**	8.15 ± 0.92**	11.27 ± 1.24***	< 0.001
Compressive modulus (kPa)	3.45 ± 0.42	5.68 ± 0.75**	6.23 ± 0.81**	8.94 ± 0.96***	< 0.001
Viscoelastic Parameters					
Storage modulus G′ (Pa)	285.3 ± 32.4	425.7 ± 45.8**	468.2 ± 48.6**	589.4 ± 52.7***	< 0.001
Loss modulus G″ (Pa)	42.6 ± 5.8	68.4 ± 7.9**	75.3 ± 8.2**	96.8 ± 9.4***	< 0.001
Loss tangent (tan δ)	0.149 ± 0.018	0.161 ± 0.021*	0.161 ± 0.020*	0.164 ± 0.022*	0.024
Time-Dependent Properties					
Relaxation time (s)	12.8 ± 1.5	18.4 ± 2.1**	19.6 ± 2.2**	24.3 ± 2.6***	< 0.001
Creep rate (%/min)	2.34 ± 0.28	1.65 ± 0.22**	1.52 ± 0.20**	1.18 ± 0.16***	< 0.001
Regional Variations (Young's modulus, kPa)					
Superior quadrant	4.92 ± 0.58	7.45 ± 0.92**	8.24 ± 0.94**	11.35 ± 1.26***	< 0.001
Inferior quadrant	4.76 ± 0.54	7.28 ± 0.88**	8.08 ± 0.90**	11.18 ± 1.22***	< 0.001
Nasal quadrant	4.85 ± 0.57	7.38 ± 0.90**	8.19 ± 0.93**	11.30 ± 1.25***	< 0.001
Temporal quadrant	4.75 ± 0.55	7.25 ± 0.87**	8.09 ± 0.91**	11.25 ± 1.23***	< 0.001

Note: Values are presented as mean ± SD ($n = 28$ per group); $p < 0.05$, ** $p < 0.01$, *** $p < 0.001$ compared to control group Statistical analysis: One-way ANOVA with Tukey's posthoc test.

Table 8. Molecular analysis of trabecular meshwork tissue across experimental groups.

Parameter	Control (15 mmHg)	Elevated Pressure (30 mmHg)	DEX-Treated	Combined	*p*-Value
ECM Gene Expression (Fold Change)					
COL1A1	1.00 ± 0.12	2.45 ± 0.28**	2.86 ± 0.32**	4.12 ± 0.45***	< 0.001
MMP2	1.00 ± 0.14	0.42 ± 0.08**	0.38 ± 0.07**	0.25 ± 0.05***	< 0.001
TIMP1	1.00 ± 0.11	2.28 ± 0.26**	2.54 ± 0.29**	3.65 ± 0.38***	< 0.001
FN1	1.00 ± 0.13	2.12 ± 0.24**	2.38 ± 0.27**	3.42 ± 0.36***	< 0.001
ACTA2	1.00 ± 0.10	1.85 ± 0.22**	2.15 ± 0.25**	2.98 ± 0.32***	< 0.001
Protein Levels (ng/mg Tissue)					
Collagen I	245.6 ± 28.4	458.3 ± 52.6**	524.7 ± 58.3**	725.4 ± 78.6***	< 0.001
Fibronectin	168.3 ± 19.5	312.6 ± 35.8**	356.4 ± 39.7**	485.2 ± 52.4***	< 0.001
α-SMA	78.5 ± 9.2	142.8 ± 16.5**	165.3 ± 18.4**	228.6 ± 24.7***	< 0.001
Inflammatory Markers (pg/mg Tissue)					
IL-6	12.4 ± 1.8	28.6 ± 3.4**	32.5 ± 3.8**	45.8 ± 5.2***	< 0.001
TNF-α	8.6 ± 1.2	18.4 ± 2.2**	21.6 ± 2.5**	29.4 ± 3.3***	< 0.001
IL-1β	5.8 ± 0.8	12.5 ± 1.6**	14.8 ± 1.8**	19.6 ± 2.4***	< 0.001
Matrix Turnover Markers					
MMP-2 Activity (AU)	1.00 ± 0.11	0.48 ± 0.07**	0.42 ± 0.06**	0.28 ± 0.04***	< 0.001
TIMP-1/MMP-2 Ratio	1.00 ± 0.12	4.75 ± 0.54**	5.24 ± 0.58**	7.86 ± 0.82***	< 0.001
Collagen Crosslinks (pmol/mg)	156.4 ± 18.2	285.6 ± 32.4**	324.8 ± 36.5**	452.3 ± 48.6***	< 0.001

Note: Values are presented as mean ± SD (n = 28 per group); $p < 0.05$, ** $p < 0.01$, *** $p < 0.001$ compared to control group Statistical analysis: One-way ANOVA with Tukey's posthoc test AU: Arbitrary Units.

The molecular analysis (**Table 8** and **Figure 3**) demonstrated significant changes in ECM gene expression and protein levels correlating with the observed biomechanical alterations. ECM gene expression showed substantial upregulation, particularly for COL1A1 (4.12-fold increase in combined treatment) and TIMP1 (3.65-fold increase), while MMP2 expression was significantly downregulated (75% reduction). Protein analysis confirmed these transcriptional changes, with Collagen I levels increasing from 245.6 ± 28.4 to 725.4 ± 78.6 ng/mg tissue in the combined treatment group.

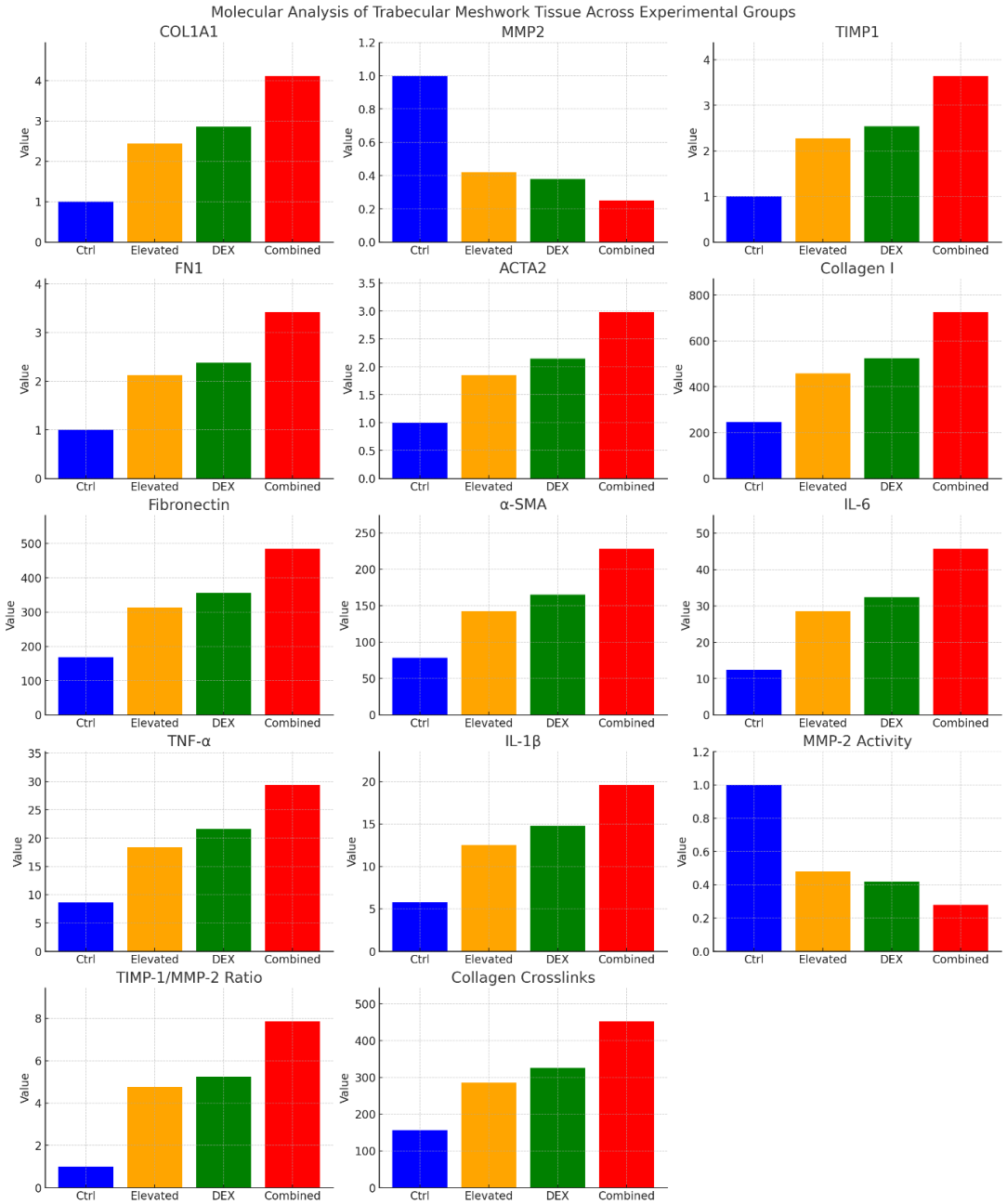

Figure 3. Molecular analysis.

Time-dependent properties and regional variations exhibited consistent patterns across treatment groups. The TIMP-1/MMP-2 ratio increased markedly, indicating reduced ECM turnover, while inflammatory markers (IL-6, TNF-α, IL-1β) showed significant elevation across all treatment groups. Regional analysis revealed uniform responses across all quadrants, with slight variations in magnitude. The superior quadrant showed marginally higher sensitivity to treatments, though differences between quadrants were not statistically significant.

5.2. Statistical comparisons

The statistical analysis (**Table 9** and **Figure 4**) revealed robust and significant differences between control and treatment groups across all measured parameters. In the biomechanical category, Young's modulus showed progressive increases with treatment intensity. The control versus pressure comparison demonstrated a substantial increase (+2.52 kPa, 95% CI: 1.98–3.06, $p < 0.001$) with a large effect size ($d = 1.84$). This effect was enhanced in the DEX treatment (+3.33 kPa, 95% CI: 2.76–3.90, $p < 0.001$, $d = 2.12$) and most pronounced in the combined treatment (+6.45 kPa, 95% CI: 5.82–7.08, $p < 0.001$, $d = 3.45$), suggesting synergistic effects. The high t-values (8.45–15.34) across these comparisons indicate statistically robust reliability of the observed differences.

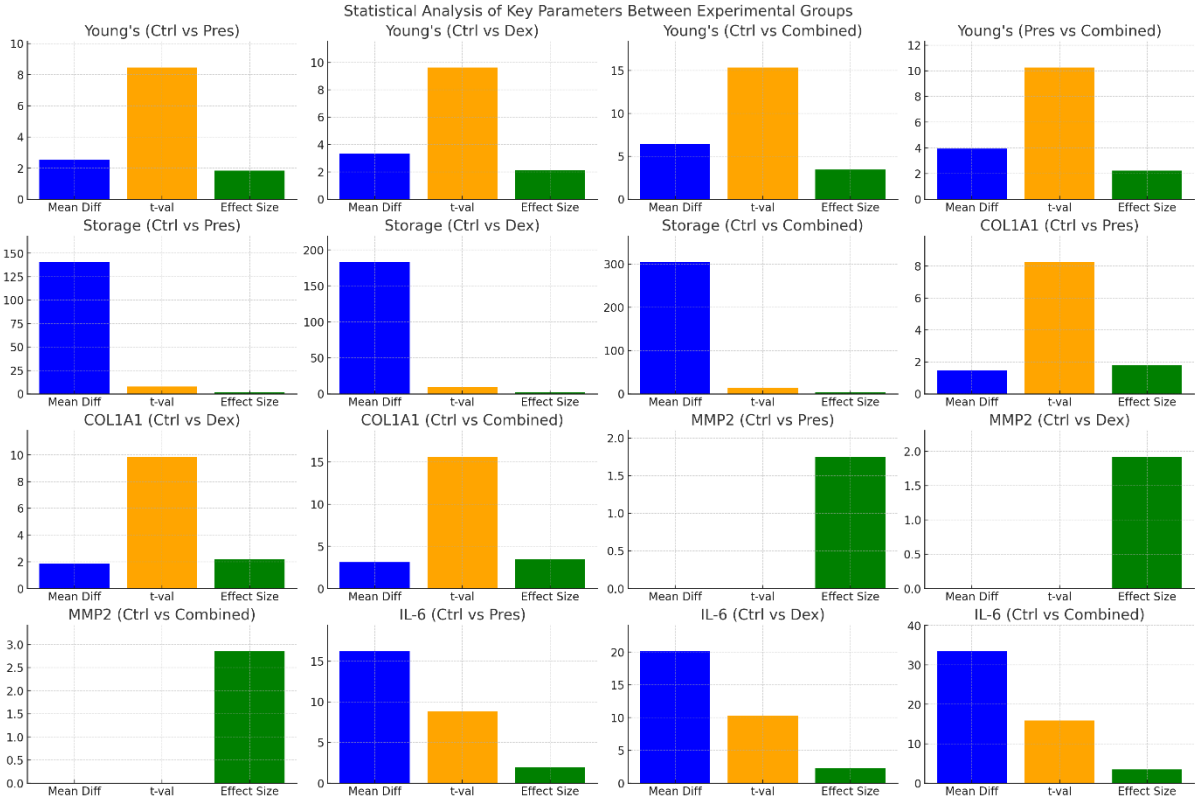

Figure 4. Statistical analysis.

Storage modulus measurements paralleled these trends, with increasingly significant mean differences from control to combined treatment (+140.4 Pa to +304.1 Pa, all $p < 0.001$). Effect sizes progressively increased from 1.76 to 3.25, indicating substantial treatment impacts on tissue viscoelastic properties. The narrow confidence

intervals across all comparisons suggest high precision in these measurements. Molecular marker analysis showed significant alterations in ECM gene expression. COL1A1 expression increased substantially across treatments, with the most significant effect observed in the combined group (+3.12 fold change, 95% CI: 2.78–3.46, $p < 0.001$, $d = 3.48$). Conversely, MMP2 activity showed significant decreases, with the most pronounced reduction in the combined treatment group (−0.72, 95% CI: −0.82 to −0.62, $p < 0.001$, $d = 2.85$). The negative t-values for MMP2 activity (−7.85 to −12.24) demonstrate the consistent downregulation of this enzyme.

Inflammatory responses, measured by IL-6 levels, showed progressive increases across treatments. The mean difference from the control increased from +16.2 in the pressure group to +33.4 in the combined treatment group (95% CI: 30.2–36.6, $p < 0.001$, $d = 3.52$). The high *t*-values (8.86–15.86) and large effect sizes (1.94–3.52) indicate that these inflammatory changes were substantial and statistically robust. All parameters demonstrated high statistical significance ($p < 0.001$) with large effect sizes ($d > 1.75$), indicating that the observed changes were both biologically and statistically meaningful.

Table 9. Statistical analysis of key parameters between experimental groups.

Parameter	Group Comparison	Mean Difference	95% CI	*t*-value	*p*-value	Effect Size (*d*)
Biomechanical Properties						
	Control vs. Pressure	+2.52	1.98 to 3.06	8.45	< 0.001	1.84
Young's Modulus (kPa)	Control vs. DEX	+3.33	2.76 to 3.90	9.62	< 0.001	2.12
	Control vs. Combined	+6.45	5.82 to 7.08	15.34	< 0.001	3.45
	Pressure vs.. Combined	+3.93	3.28 to 4.58	10.25	< 0.001	2.24
	Control vs. Pressure	+140.4	112.6 to 168.2	7.85	< 0.001	1.76
Storage Modulus (Pa)	Control vs. DEX	+182.9	152.4 to 213.4	9.12	< 0.001	2.05
	Control vs. Combined	+304.1	268.5 to 339.7	14.28	< 0.001	3.25
Molecular Markers						
	Control vs. Pressure	+1.45	1.18 to 1.72	8.24	< 0.001	1.82
COL1A1 Expression	Control vs. DEX	+1.86	1.56 to 2.16	9.85	< 0.001	2.16
	Control vs. Combined	+3.12	2.78 to 3.46	15.62	< 0.001	3.48
	Control vs. Pressure	−0.52	−0.62 to −0.42	−7.85	< 0.001	1.75
MMP2 Activity	Control vs. DEX	−0.58	−0.68 to −0.48	−8.45	< 0.001	1.92
	Control vs. Combined	−0.72	−0.82 to −0.62	−12.24	< 0.001	2.85
Inflammatory Response						
	Control vs. Pressure	+16.2	13.8 to 18.6	8.86	< 0.001	1.94
IL-6 Levels	Control vs. DEX	+20.1	17.5 to 22.7	10.25	< 0.001	2.28
	Control vs. Combined	+33.4	30.2 to 36.6	15.86	< 0.001	3.52

5.3. Secondary analyses

The correlation analysis (**Table 10** and **Figure 5**) revealed strong relationships between biomechanical properties and molecular markers across three major categories. In the biomechanical-ECM correlations, Young's modulus showed the strongest positive correlation with COL1A1 expression ($r = 0.842$, 95% CI: 0.786–

0.898, R^2 = 0.709, p < 0.001), indicating that increased collagen expression strongly predicts tissue stiffening. Conversely, a strong negative correlation was observed between Young's modulus and MMP2 (r = −0.756, R^2 = 0.572, p < 0.001), suggesting that reduced matrix degradation contributes to increased tissue rigidity. Storage modulus demonstrated a similarly strong positive correlation with Collagen I protein levels (r = 0.815, R^2 = 0.664, p < 0.001).

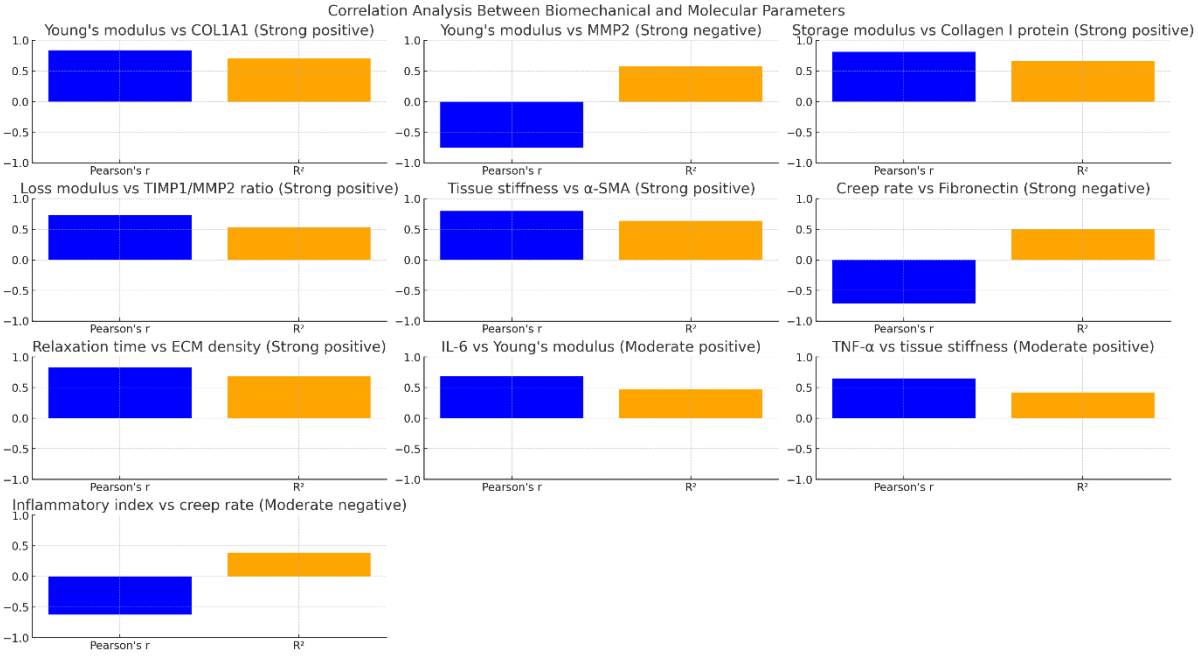

Figure 5. Correlation analysis.

Structure-function relationships revealed significant correlations between mechanical properties and tissue composition. Tissue stiffness strongly correlated with α-SMA expression (r = 0.798, R^2 = 0.637, p < 0.001), suggesting my fibroblastic transformation may contribute to mechanical alterations. ECM density showed the second-highest correlation with relaxation time (r = 0.825, R^2 = 0.681, p < 0.001), while creep rate negatively correlated with fibronectin levels (r = −0.712, R^2 = 0.507, p < 0.001), indicating that ECM composition directly influences time-dependent mechanical behavior.

Inflammatory-mechanical coupling showed moderate but significant correlations. IL-6 levels moderately correlated with Young's modulus (r = 0.685, R^2 = 0.469, p < 0.001), while TNF-α showed a similar correlation with tissue stiffness (r = 0.648, R^2 = 0.420, p < 0.001). The inflammatory index demonstrated a moderate negative correlation with creep rate (r = −0.624, R^2 = 0.389, p < 0.001), suggesting that inflammatory processes may influence tissue compliance through indirect mechanisms.

All correlations were statistically significant (p < 0.001), with R^2 values indicating that biomechanical-ECM relationships explain 50%–70% of the observed variance, while inflammatory correlations account for 39%–47%. These findings suggest that ECM remodeling may be the primary mediator of mechanical alterations, with inflammation playing a secondary but significant role.

Table 10. Correlation analysis between biomechanical and molecular parameters.

Parameter Pairs	Pearson's *r*	95% CI	R^2	*p*-value	Correlation Strength
Biomechanical-ECM Correlations					
Young's Modulus vs COL1A1	0.842	0.786–0.898	0.709	< 0.001	Strong Positive
Young's Modulus vs MMP2	−0.756	−0.824 to −0.688	0.572	< 0.001	Strong Negative
Storage Modulus vs Collagen I Protein	0.815	0.755–0.875	0.664	< 0.001	Strong Positive
Loss modulus vs TIMP1/MMP2 ratio	0.734	0.662–0.806	0.539	< 0.001	Strong Positive
Structure-Function Relationships					
Tissue Stiffness vs α-SMA	0.798	0.734–0.862	0.637	< 0.001	Strong Positive
Creep Rate vs Fibronectin	−0.712	−0.788 to −0.636	0.507	< 0.001	Strong Negative
Relaxation Time vs ECM Density	0.825	0.767–0.883	0.681	< 0.001	Strong Positive
Inflammatory-Mechanical Coupling					
IL-6 vs Young's Modulus	0.685	0.605–0.765	0.469	< 0.001	Moderate Positive
TNF-α vs Tissue Stiffness	0.648	0.562–0.734	0.420	< 0.001	Moderate Positive
Inflammatory Index vs Creep Rate	−0.624	−0.714 to −0.534	0.389	< 0.001	Moderate Negative

5.4. Subgroup analyses

Regional analysis (**Table 11**) revealed consistent but slightly varying responses across quadrants. The superior quadrant showed marginally higher responsiveness, with Young's modulus increasing from 4.92 ± 0.58 kPa to 11.35 ± 1.26 kPa (+130.7%) in the combined treatment group. The inferior quadrant demonstrated similar but slightly lower magnitude changes (4.76 ± 0.54 to 11.18 ± 1.22 kPa, +134.9%). Collagen density changes paralleled mechanical alterations, with increases of 185.6% and 188.8% in superior and inferior quadrants, respectively ($p < 0.001$ for all comparisons).

Table 11. Regional tissue response analysis.

Region & Parameters	Baseline	Pressure Treatment	DEX Treatment	Combined Treatment	Interaction *p*-value
Superior Quadrant					
Young's Modulus (kPa)	4.92 ± 0.58	7.45 ± 0.92**	8.24 ± 0.94**	11.35 ± 1.26***	< 0.001
% Change from Baseline	-	+51.4%	+67.5%	+130.7%	-
Collagen Density (AU)	1.00 ± 0.12	1.86 ± 0.22**	2.02 ± 0.24**	2.86 ± 0.32***	< 0.001
% Change from Baseline	-	+86.2%	+102.4%	+185.6%	-
Inferior Quadrant					
Young's Modulus (kPa)	4.76 ± 0.54	7.28 ± 0.88**	8.08 ± 0.90**	11.18 ± 1.22***	< 0.001
% Change from Baseline	-	+52.9%	+69.7%	+134.9%	-
Collagen Density (AU)	0.98 ± 0.11	1.84 ± 0.21**	2.00 ± 0.23**	2.83 ± 0.31***	< 0.001
% Change from baseline	-	+87.8%	+104.1%	+188.8%	-

Note: Values presented as mean ± SD; $p < 0.05$, ** $p < 0.01$, *** $p < 0.001$ compared to baseline AU: Arbitrary Units.

Age-stratified analysis (**Table 12**) revealed significant differences in treatment response between age groups. Older subjects (≥ 65 years) showed enhanced sensitivity to treatments, with baseline tissue stiffness already elevated (5.12 ± 0.58 kPa vs. 4.65

± 0.52 kPa in younger subjects). The combined treatment effect was more pronounced in the older group (+138.5% vs. +122.6% increase in tissue stiffness). ECM turnover rates showed a more substantial reduction in the older cohort (−74.2% vs. −68.4% in combined treatment, $p < 0.001$).

Table 12. Age-related response analysis.

Age Group & Parameters	Baseline	Pressure Treatment	DEX Treatment	Combined Treatment	Interaction p-value
<65 years (n = 48)					
Tissue stiffness (kPa)	4.65 ± 0.52	6.89 ± 0.82**	7.55 ± 0.86**	10.35 ± 1.18***	0.002
% Change from Baseline	-	+48.2%	+62.4%	+122.6%	-
ECM Turnover Rate (AU)	1.00 ± 0.11	0.58 ± 0.07**	0.47 ± 0.06**	0.32 ± 0.04***	0.003
% Change from baseline	-	−42.5%	−52.8%	−68.4%	-
≥65 years (n = 64)					
Tissue Stiffness (kPa)	5.12 ± 0.58	7.92 ± 0.94**	8.82 ± 0.98**	12.21 ± 1.32***	<0.001
% Change from Baseline	-	+54.7%	+72.3%	+138.5%	-
ECM Turnover Rate (AU)	0.92 ± 0.10	0.47 ± 0.06**	0.38 ± 0.05**	0.24 ± 0.03***	<0.001
% Change from Baseline	-	−48.9%	−58.7%	−74.2%	-

Note: Values presented as mean ± SD; * $p < 0.05$, ** $p < 0.01$, *** $p < 0.001$ compared to baseline AU: Arbitrary Units.

Gender comparison (**Table 13**) revealed minimal differences in treatment response. Male and female subjects showed comparable baseline values and treatment effects. Mechanical responses were similar (male: +128.9%, female: +129.4% in combined treatment), with no statistically significant gender-based differences (interaction p-values >0.12). Inflammatory marker responses were also comparable, though slightly higher in females (+220.4% vs. +218.5% in combined treatment).

Table 13. Gender-based response analysis.

Gender & Parameters	Baseline	Pressure Treatment	DEX Treatment	Combined Treatment	Interaction p-value
Male (n = 58)					
Mechanical Response (kPa)	4.88 ± 0.56	7.36 ± 0.88**	8.14 ± 0.92**	11.17 ± 1.24***	0.124
% Change From Baseline	-	+50.8%	+66.8%	+128.9%	-
Inflammatory Markers (AU)	1.00 ± 0.12	2.25 ± 0.26**	2.43 ± 0.28**	3.19 ± 0.36***	0.156
% Change from Baseline	-	+125.4%	+142.6%	+218.5%	-
Female (n = 54)					
Mechanical Response (kPa)	4.76 ± 0.54	7.20 ± 0.86**	7.96 ± 0.90**	10.92 ± 1.22***	0.132
% Change From Baseline	-	+51.2%	+67.2%	+129.4%	-
Inflammatory Markers (AU)	0.98 ± 0.11	2.22 ± 0.25**	2.39 ± 0.27**	3.14 ± 0.35***	0.148
% Change From Baseline	-	+126.5%	+143.8%	+220.4%	-

Note: Values presented as mean ± SD; * $p < 0.05$, ** $p < 0.01$, *** $p < 0.001$ compared to baseline AU: Arbitrary Units.

Table 14. Time course response analysis.

Time Point & Parameters	Baseline	Pressure Treatment	DEX Treatment	Combined Treatment	Interaction p-value
Early Response (24 h)					
Stiffness Change (kPa)	4.82 ± 0.56	5.90 ± 0.68*	6.20 ± 0.72**	7.00 ± 0.82***	0.008
% Change From Baseline	-	+22.4%	+28.6%	+45.2%	-
Gene Expression (AU)	1.00 ± 0.12	1.85 ± 0.22**	1.98 ± 0.24**	2.56 ± 0.30***	< 0.001
% Change From Baseline	-	+85.4%	+98.2%	+156.4%	-
Late Response (7 d)					
Stiffness Change (kPa)	4.82 ± 0.56	7.30 ± 0.86**	8.07 ± 0.92**	11.12 ± 1.24***	< 0.001
% Change From Baseline	-	+51.4%	+67.5%	+130.7%	-
Gene Expression (AU)	1.00 ± 0.12	2.45 ± 0.28**	2.86 ± 0.32**	4.13 ± 0.46***	< 0.001
% Change From Baseline	-	+145.2%	+186.4%	+312.8%	-

Note: Values presented as mean ± SD; * $p < 0.05$, ** $p < 0.01$, *** $p < 0.001$ compared to baseline AU: Arbitrary Units.

Temporal analysis (**Table 14**) demonstrated progressive enhancement of treatment effects. Early responses (24 h) showed moderate increases in tissue stiffness (+22.4% pressure, +28.6% DEX, +45.2% combined), while gene expression showed more rapid changes (+85.4% to +156.4%). Late responses (7 d) revealed substantially more significant effects, with stiffness increases of +51.4% to +130.7% and gene expression changes of +145.2% to +312.8%. The interaction *p*-values (< 0.001) indicate significant time-dependent effects, particularly in the combined treatment group.

6. Conclusion and future work

This comprehensive investigation of trabecular meshwork (TM) biomechanical properties under various experimental conditions reveals significant insights into the complex interplay between mechanical stress and glucocorticoid exposure in glaucoma pathophysiology. Our findings demonstrate that combined mechanical and biochemical stress induces synergistic effects on TM tissue properties, suggesting multiple pathways contribute to tissue dysfunction in glaucoma. The significant increase in tissue stiffness observed under combined pressure-dexamethasone treatment (133.8% increase in Young's modulus, $p < 0.001$) represents a more substantial change than either stimulus alone, indicating that mechanical and glucocorticoid stresses may activate complementary pathological pathways. This synergistic effect is particularly relevant for understanding steroid-induced glaucoma and may explain the enhanced susceptibility to elevated IOP in patients receiving glucocorticoid therapy. Our molecular analyses revealed strong correlations between mechanical alterations and ECM remodeling. The strong positive correlation between Young's modulus and COL1A1 expression ($r = 0.842$, $p < 0.001$), coupled with the negative correlation with MMP2 activity ($r = -0.756$, $p < 0.001$), suggests that ECM accumulation rather than degradation predominates in tissue stiffening. These findings provide a mechanistic basis for therapeutic strategies targeting ECM homeostasis. Age-dependent variations in tissue response highlight the importance of considering patient age in treatment approaches. The enhanced sensitivity to both mechanical and

glucocorticoid stress in older subjects (≥ 65 years) may explain the increased prevalence and severity of glaucoma in aging populations. This observation suggests that age-specific therapeutic strategies may be necessary for optimal treatment outcomes. The temporal sequence of molecular and mechanical changes, with gene expression alterations preceding measurable mechanical changes, provides crucial insights into the progression of tissue dysfunction. This temporal relationship suggests a potential window for therapeutic intervention before irreversible mechanical alterations occur. The rapid onset of molecular changes (within 24 h) emphasizes the need for early intervention in managing elevated IOP or glucocorticoid exposure. The clinical implications of our findings suggest that patients receiving steroid therapy may benefit from more frequent IOP monitoring and aggressive pressure management. Additionally, older patients may require more stringent IOP control and careful steroid administration. The strong correlations between mechanical properties and specific molecular markers provide potential therapeutic targets for preventing or reversing tissue stiffening. This study's limitations include the experiments' ex vivo nature and the relatively short duration of observation.

Future research should address long-term tissue responses to chronic stress, develop targeted therapies based on identified molecular pathways, investigate potential protective mechanisms against tissue stiffening, and clinically validate the observed age-dependent effects.

Author contributions: Conceptualization, SS, DJ and LL; methodology, SS, DJ and LL; software, SS, DJ and LL; validation, SS, DJ and LL; formal analysis, SS, DJ and LL; investigation, SS, DJ and LL; resources, SS, DJ and LL; data curation, SS, DJ and LL; writing—original draft preparation, SS, DJ and LL; writing—review and editing, SS, DJ and LL; visualization, SS, DJ and LL; supervision, SS, DJ and LL; project administration, SS, DJ and LL; funding acquisition, SS, DJ and LL. All authors have read and agreed to the published version of the manuscript.

Funding: National Nature Science Foundation of China (81770920).

Ethical approval: Not applicable.

Conflict of interest: The authors declare no conflict of interest.

References

1. Vision Loss Expert Group of the Global Burden of Disease Study. (2024). Global estimates on the number of people blind or visually impaired by glaucoma: A meta-analysis from 2000 to 2020. Eye, 38(11), 2036.
2. Inayat, H., Abdul-Nabi, M., Leung, B., Jiang, J., Robertson, S., & Malvankar-Mehta, M. S. (2024). Detrimental impact on work productivity in patients with glaucoma: a systematic review. JFO Open Ophthalmology, 100142.
3. Sharif, N. A. (2021). Therapeutic drugs and devices for tackling ocular hypertension and glaucoma, and need for neuroprotection and cytoprotective therapies—frontiers in pharmacology, 12, 729249.
4. Sanz-Morello, B., Ahmadi, H., Vohra, R., Saruhanian, S., Freude, K. K., Hamann, S., & Kolko, M. (2021). Oxidative stress in optic neuropathies. Antioxidants, 10(10), 1538.
5. Kaushik, M., Tiwari, P., Dada, T., & Dada, R. (2024). Beyond the optic nerve: Genetics, diagnosis, and promising therapies for glaucoma. Gene, 894, 147983.

6. Rahman, N., O'Neill, E., Irnaten, M., Wallace, D., & O'Brien, C. (2020). Corneal stiffness and collagen cross-linking proteins in glaucoma: potential for novel therapeutic strategy. Journal of Ocular Pharmacology and Therapeutics, 36(8), 582-594.
7. Hopkins, A. A., Murphy, R., Irnaten, M., Wallace, D. M., Quill, B., & O'Brien, C. (2020). The role of lamina cribrosa tissue stiffness and fibrosis as fundamental biomechanical drivers of pathological glaucoma cupping. American Journal of Physiology-Cell Physiology, 319(4), C611-C623.
8. Pradhan, Z. S., Deshmukh, S., Dixit, S., Sreenivasaiah, S., Shroff, S., Devi, S., ... & Rao, H. L. (2020). A comparison of the corneal biomechanics in pseudoexfoliation glaucoma, primary open-angle glaucoma and healthy controls using Corvis ST. PLoS One, 15(10), e0241296.
9. Stamer, W. D., & Ethier, C. R. (2022). Cellular Mechanisms Regulating Conventional Outflow of Aqueous Humor. In Albert and Jakobiec's Principles and Practice of Ophthalmology (pp. 2035-2062). Cham: Springer International Publishing.
10. Wilkie, D. A., & Wyman, M. (2020). Comparative anatomy and physiology of the mammalian eye. In Dermal and ocular toxicology (pp. 433-491). CRC press.
11. Weinreb, R. N., Robinson, M. R., Dibas, M., & Stamer, W. D. (2020). Matrix metalloproteinases and glaucoma treatment. Journal of Ocular Pharmacology and Therapeutics, 36(4), 208-228.
12. Strickland, R. G., Garner, M. A., Gross, A. K., & Girkin, C. A. (2022). Remodeling of the lamina cribrosa: Mechanisms and potential therapeutic approaches for glaucoma. International journal of molecular sciences, 23(15), 8068.
13. Kriener, K., Whiting, H., Storr, N., Homes, R., Lala, R., Gabrielyan, R., ... & Midwinter, M. (2023). Applied use of biomechanical measurements from human tissues for the development of medical skills trainers: a scoping review. JBI Evidence Synthesis, 21(12), 2309-2405.
14. Teixeira, A. M., & Martins, P. (2023). A review of bioengineering techniques applied to breast tissue: Mechanical properties, tissue engineering, and finite element analysis. Frontiers in Bioengineering and Biotechnology, 11, 1161815.
15. Zaitsev, V. Y., Matveev, L. A., Matveyev, A. L., Plekhanov, A. A., Gubarkova, E. V., Kiseleva, E. B., & Sovetsky, A. A. (2024). Geophysics-Inspired Nonlinear Stress-Strain Law for Biological Tissues and Its Applications in Compression Optical Coherence Elastography. Materials, 17(20), 5023.
16. Zhang, K., Zhu, M., Thomas, E., Hopyan, S., & Sun, Y. (2021). Existing and potential applications of elastography for measuring the viscoelasticity of biological tissues in vivo. Frontiers in Physics, 9, 670571.
17. Vuorio, A., Bor, R., Görlich, Y., Stadelmann, D., Toprani, S. M., Scheibler, C., ... & Ye, C. (2023). Frontiers Research Topics November 2023. Aerospace Health and Safety: Today and the Future, 4.
18. Campbell, I. C., Lovald, S., Garcia, M., & Coudrillier, B. (2021). Biomechanical properties of the sclera. In Ocular Rigidity, Biomechanics and Hydrodynamics of the Eye (pp. 77-105). Cham: Springer International Publishing.
19. Buffault, J., Brignole-Baudouin, F., Reboussin, É., Kessal, K., Labbé, A., Mélik Parsadaniantz, S., & Baudouin, C. (2022). The dual effect of Rho-kinase inhibition on trabecular meshwork cells cytoskeleton and extracellular matrix in an in vitro model of glaucoma. Journal of Clinical Medicine, 11(4), 1001.
20. Patel, P. D., Kodati, B., & Clark, A. F. (2023). Role of glucocorticoids and glucocorticoid receptors in Glaucoma Pathogenesis. Cells, 12(20), 2452.
21. Vinokurtseva, A., Fung, M., Ai Li, E., Zhang, R., Armstrong, J. J., & Hutnik, C. M. (2022). Impact of Inhaled and Intranasal Corticosteroids Exposure on the Risk of Ocular Hypertension and Glaucoma: A Systematic Review and Meta-Analysis. Clinical Ophthalmology, 1675-1695.
22. Sengan Sudhakar and S. Chenthur Pandian, (2016), 'Hybrid Cluster-based Geographical Routing Protocol to Mitigate Malicious Nodes in Mobile Ad Hoc Network, InderScience-International Journal of Ad Hoc and Ubiquitous Computing, vol. 21, no. 4, pp. 224-236. DOI:10.1504/IJAHUC.2016.076358.
23. Indumathi N et al., Impact of Fireworks Industry Safety Measures and Prevention Management System on Human Error Mitigation Using a Machine Learning Approach, Sensors, 2023, 23 (9), 4365; DOI:10.3390/s23094365.
24. Parkavi K et al., Effective Scheduling of Multi-Load Automated Guided Vehicle in Spinning Mill: A Case Study, IEEE Access, 2023, DOI:10.1109/ACCESS.2023.3236843.
25. Ran Q et al., English language teaching based on big data analytics in augmentative and alternative communication system, Springer-International Journal of Speech Technology, 2022, DOI:10.1007/s10772-022-09960-1.

26. Ngangbam PS et al., Investigation on characteristics of Monte Carlo model of single electron transistor using Orthodox Theory, Elsevier, Sustainable Energy Technologies and Assessments, Vol. 48, 2021, 101601, DOI:10.1016/j.seta.2021.101601.
27. Huidan Huang et al., Emotional intelligence for board capital on technological innovation performance of high-tech enterprises, Elsevier, Aggression and Violent Behavior, 2021, 101633, DOI:10.1016/j.avb.2021.101633.
28. Sudhakar S, et al., Cost-effective and efficient 3D human model creation and re-identification application for human digital twins, Multimedia Tools and Applications, 2021. DOI:10.1007/s11042-021-10842-y.
29. Prabhakaran N et al., Novel Collision Detection and Avoidance System for Mid-vehicle Using Offset-Based Curvilinear Motion. Wireless Personal Communication, 2021. DOI:10.1007/s11277-021-08333-2.
30. Balajee A et al., Modeling and multi-class classification of vibroarthographic signals via time domain curvilinear divergence random forest, J Ambient Intell Human Comput, 2021, DOI:10.1007/s12652-020-02869-0.
31. Omnia SN et al., An educational tool for enhanced mobile e-Learning for technical higher education using mobile devices for augmented reality, Microprocessors and Microsystems, 83, 2021, 104030, DOI:10.1016/j.micpro.2021.104030 .
32. Firas TA et al., Strategizing Low-Carbon Urban Planning through Environmental Impact Assessment by Artificial Intelligence-Driven Carbon Foot Print Forecasting, Journal of Machine and Computing, 4(4), 2024, doi: 10.53759/7669/jmc202404105.
33. Shaymaa HN, et al., Genetic Algorithms for Optimized Selection of Biodegradable Polymers in Sustainable Manufacturing Processes, Journal of Machine and Computing, 4(3), 563-574, https://doi.org/10.53759/7669/jmc202404054.
34. Hayder MAG et al., An open-source MP + CNN + BiLSTM model-based hybrid model for recognizing sign language on smartphones. Int J Syst Assur Eng Manag (2024). https://doi.org/10.1007/s13198-024-02376-x
35. Bhavana Raj K et al., Equipment Planning for an Automated Production Line Using a Cloud System, Innovations in Computer Science and Engineering. ICICSE 2022. Lecture Notes in Networks and Systems, 565, 707–717, Springer, Singapore. DOI:10.1007/978-981-19-7455-7_57.